Spontaneous emission of a cesium atom near a nanofiber: Efficient coupling of light to guided modes

Fam Le Kien,[1,*] S. Dutta Gupta,[1,2] V. I. Balykin,[1,3] and K. Hakuta[1]
[1]*Department of Applied Physics and Chemistry, University of Electro-Communications, Chofu, Tokyo 182-8585, Japan*
[2]*School of Physics, University of Hyderabad, Hyderabad, India*
[3]*Institute of Spectroscopy, Troitsk, Moscow Region, 142092, Russia*
(Received 16 June 2005; published 28 September 2005; publisher error corrected 3 October 2005)

We study the spontaneous emission of a cesium atom in the vicinity of a subwavelength-diameter fiber. We show that the confinement of the guided modes and the degeneracy of the excited and ground states substantially affect the spontaneous emission process. We demonstrate that different magnetic sublevels have different decay rates. When the fiber radius is about 200 nm, a significant fraction (up to 28%) of spontaneous emission by the atom can be channeled into guided modes. Our results may find applications for developing nanoprobes for atoms and efficient couplers for subwavelength-diameter fibers.

DOI: 10.1103/PhysRevA.72.032509 PACS number(s): 32.30.Jc, 32.70.Jz, 32.80.Pj, 03.75.Be

I. INTRODUCTION

Coupling of light to subwavelength structures and its control pose one of the greatest challenges of recent research [1]. In this paper, we show how such coupling with efficiency of up to 28% can be achieved in a realistic system of a cesium atom near a subwavelength-diameter fiber. Note that modification of the vacuum near the fiber and its effect on the spontaneous emission has been studied in the context of two-level atoms [2–4]. Many other studies exist involving other geometries [5,6]. Most of these investigations, to the best of our knowledge, do not go beyond the two-level approximation for the atom. The inclusion of hyperfine structure of the atom can significantly affect the actual rate of spontaneous decay. Some parameters that describe the decay of cross-level coherences arise only in the framework of a multilevel-atom model. The knowledge of both diagonal and off-diagonal types of decay characteristics is required for the studies of absorption and emission properties, optical response, and dynamical behavior of realistic atoms [7]. We show that the confinement of the guided modes and the degeneracy of the excited and ground states substantially affect the spontaneous emission process. We find that different magnetic sublevels have different decay rates. We demonstrate that the thin fiber can indeed act as a subwavelength probe, since about one fourth of the spontaneous emission from the atom can be channeled into guided modes. The knowledge of spontaneous emission characteristics is important yet from the angle of atom optics [8], in particular, from design considerations of atom traps [9]. A recent proposal for *microscopic* trapping of individual atoms involves the use of a subwavelength-diameter silica fiber with a single (red-detuned) [10] or two (red- and blue-detuned) light beams [11] launched into it.

The paper is organized as follows. In Sec. II we describe the model. In Sec. III we derive the basic characteristics of spontaneous emission for the model. In Sec. IV we present numerical results. Our conclusions are given in Sec. V.

II. MODEL

We consider a cesium atom trapped in the vicinity of a subwavelength-diameter silica fiber (see the upper part of Fig. 1). We use the fiber axis z as the quantization axis for atomic states. For atoms trapped in a magneto-optical trap, the quantization axis can be specified and hence controlled by the direction of the magnetic field in the trap. We study the cesium D_2 line, which occurs at the wavelength $\lambda_0 = 852$ nm and corresponds to the transition from the excited state $6P_{3/2}$ to the ground state $6S_{1/2}$ (see the lower part of Fig. 1). We assume that the atom is initially prepared in the hyperfine-structure (hfs) level $F'=5$ of the state $6P_{3/2}$. We

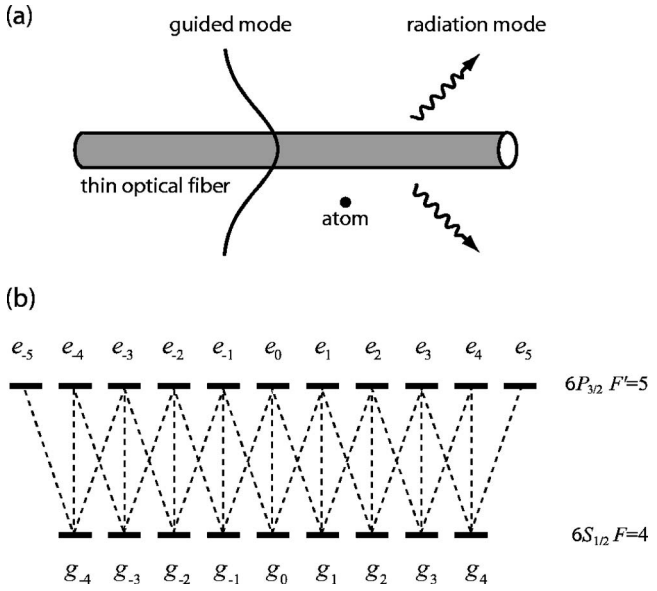

FIG. 1. (a) An atom interacting with guided and radiation modes in the vicinity of a thin optical fiber. (b) Schematic of the $6P_{3/2}F'=5$ and $6S_{1/2}F=4$ hfs levels of a cesium atom.

*Also at Institute of Physics and Electronics, Vietnamese Academy of Science and Technology, Hanoi, Vietnam.

introduce the notation $e_{M'}$ and g_M for the magnetic sublevels $F'M'$ and FM of the hfs levels $6P_{3/2}F'=5$ and $6S_{1/2}F=4$, respectively. Due to the selection rule, spontaneous emission from the hfs level $6P_{3/2}F'=5$ to the ground state is always to the hfs level $6S_{1/2}F=4$, not to the hfs level $6S_{1/2}F=3$. Therefore, the magnetic sublevels $e_{M'}$ and g_M of the hfs levels $6P_{3/2}F'=5$ and $6S_{1/2}F=4$, respectively, form a closed set, which is used for laser cooling in magneto-optical traps [12]. The coupling between $e_{M'}$ and g_M by spontaneous emission is illustrated in the lower part of Fig. 1.

In the interaction picture, the atomic dipole operator is given by

$$\mathbf{D}=\sum_{eg}(\mathbf{d}_{eg}^{*}\sigma_{ge}e^{-i\omega_0 t}+\mathbf{d}_{eg}\sigma_{ge}^{\dagger}e^{i\omega_0 t}). \tag{1}$$

Here, the operators $\sigma_{ge}=|g\rangle\langle e|$ and $\sigma_{ge}^{\dagger}=\sigma_{eg}=|e\rangle\langle g|$ describe the downward and upward transitions, respectively, and $\mathbf{d}_{eg}=\langle e|\mathbf{D}|g\rangle e^{-i\omega_0 t}$ is the dipole matrix element. We introduce the notation $d^{(-1)}=(d_x-id_y)/\sqrt{2}$, $d^{(0)}=d_z$, and $d^{(1)}=-(d_x+id_y)/\sqrt{2}$ for the spherical tensor components of the dipole vector $\mathbf{d}$. We label the spherical tensor components by the index $l=0,\pm 1$. The l spherical component of the dipole moment for the transition between $e_{M'}$ and g_M is given by [13]

$$d_{e_{M'}g_M}^{(l)}=(-1)^{I+J'-M'}\langle J'\|D\|J\rangle\sqrt{(2F+1)(2F'+1)}\times\begin{Bmatrix}J' & F' & I\\ F & J & 1\end{Bmatrix}\begin{pmatrix}F & 1 & F'\\ M & l & -M'\end{pmatrix}, \tag{2}$$

where the array in the curly braces is a $6j$ symbol, the array in the parentheses is a $3j$ symbol, J is the total electronic angular momentum, I is the nuclear spin, F is total atomic angular momentum, M is the magnetic quantum number, and $\langle J'\|D\|J\rangle$ is the reduced electric-dipole matrix element in the J basis.

We assume that the fiber has a cylindrical silica core of radius a and refractive index n_1 and an infinite vacuum clad of refractive index $n_2=1$. We retain the silica dispersion and at the frequency of the cesium D_2 line the refractive index n_1 of the fiber is taken as 1.45. The positive-frequency part $\mathbf{E}^{(+)}$ of the electric component of the field can be decomposed into the contributions from the guided and radiation modes as

$$\mathbf{E}^{(+)}=\mathbf{E}_{\text{guided}}^{(+)}+\mathbf{E}_{\text{rad}}^{(+)}. \tag{3}$$

We do not take into account the evanescent modes, which do not contribute to the spontaneous emission process [3]. We use the cylindrical coordinates (r,φ,z) with z as the axis of the fiber. In view of the very low losses of silica in the wavelength range of interest, we neglect material absorption.

The continuum field quantization follows the procedures presented in Ref. [14]. Regarding the guided modes, we assume that the single-mode condition [15] is satisfied for a finite bandwidth of the field frequency ω around the cesium D_2-line frequency ω_0. We label each guided mode by an index $\mu=(\omega,f,p)$, where $f=+,-$ denotes forward or backward propagation direction, and $p=+,-$ denotes the counterclockwise or clockwise rotation of polarization. When we quantize the field in the guided modes, we obtain the following expression for $\mathbf{E}_{\text{guided}}^{(+)}$ in the interaction picture:

$$\mathbf{E}_{\text{guided}}^{(+)}=i\sum_{fp}\int_0^{\infty}d\omega\sqrt{\frac{\hbar\omega\beta'}{4\pi\epsilon_0}}a_{\mu}\mathbf{e}^{(\mu)}e^{-i(\omega t-f\beta z-p\varphi)}. \tag{4}$$

Here β is the longitudinal propagation constant, β' is the derivative of β with respect to ω, a_{μ} is the respective photon annihilation operator, and $\mathbf{e}^{(\mu)}=\mathbf{e}^{(\mu)}(r,\varphi)$ is the electric-field profile function of the guided mode μ in the classical problem. The constant β is determined by the fiber eigenvalue equation [15]. The operators a_{μ} and $a_{\mu}^{\dagger}$ satisfy the continuous-mode bosonic commutation rules $[a_{\mu},a_{\mu'}^{\dagger}]=\delta(\omega-\omega')\delta_{ff'}\delta_{pp'}$. The mode function $\mathbf{e}^{(\mu)}$ is given in Ref. [15] (see Appendix A). The normalization of $\mathbf{e}^{(\mu)}$ is given by

$$\int_0^{2\pi}d\varphi\int_0^{\infty}n_{\text{rf}}^2|\mathbf{e}^{(\mu)}|^2rdr=1. \tag{5}$$

Here $n_{\text{rf}}(r)=n_1$ for $r<a$, and $n_{\text{rf}}(r)=n_2$ for $r>a$.

Unlike the case of guided modes, in the case of radiation modes, the longitudinal propagation constant β for each value of ω can vary continuously, from $-kn_2$ to kn_2 (with $k=\omega/c$). We label each radiation mode by the index $\nu=(\omega,\beta,m,p)$, where m is the mode order and p is the mode polarization. When we quantize the field in the radiation modes, we obtain the following expression for $\mathbf{E}_{\text{rad}}^{(+)}$ in the interaction picture:

$$\mathbf{E}_{\text{rad}}^{(+)}=i\sum_{mp}\int_0^{\infty}d\omega\int_{-kn_2}^{kn_2}d\beta\sqrt{\frac{\hbar\omega}{4\pi\epsilon_0}}a_{\nu}\mathbf{e}^{(\nu)}e^{-i(\omega t-\beta z-m\varphi)}. \tag{6}$$

Here a_{ν} is the respective photon annihilation operator, and $\mathbf{e}^{(\nu)}=\mathbf{e}^{(\nu)}(r,\varphi)$ is the electric-field profile function of the radiation mode ν in the classical problem. The operators a_{ν} and $a_{\nu}^{\dagger}$ satisfy the continuous-mode bosonic commutation rules $[a_{\nu},a_{\nu'}^{\dagger}]=\delta(\omega-\omega')\delta(\beta-\beta')\delta_{mm'}\delta_{pp'}$. The mode function $\mathbf{e}^{(\nu)}$ is given in Ref. [15] (see Appendix B). The normalization of $\mathbf{e}^{(\nu)}$ is given by

$$\int_0^{2\pi}d\varphi\int_0^{\infty}n_{\text{rf}}^2[\mathbf{e}^{(\nu)}\mathbf{e}^{(\nu')*}]_{\beta=\beta',m=m',p=p'}rdr=\delta(\omega-\omega'). \tag{7}$$

Assume that the atom is located at a point (r,φ,z). The Hamiltonian for the atom-field interaction in the dipole and rotating-wave approximations is given by

$$H_{\text{int}}=-i\hbar\sum_{fpeg}\int_0^{\infty}d\omega\,G_{\mu eg}\sigma_{ge}^{\dagger}a_{\mu}e^{-i(\omega-\omega_0)t}-i\hbar\sum_{mpeg}\int_0^{\infty}d\omega\int_{-kn_2}^{kn_2}d\beta\,G_{\nu eg}\sigma_{ge}^{\dagger}a_{\nu}e^{-i(\omega-\omega_0)t}+\text{H.c.}. \tag{8}$$

Here the coefficients $G_{\mu eg}$ and $G_{\nu eg}$ characterize the coupling of the atomic transition $e\leftrightarrow g$ with the guided mode

$\mu=(\omega,f,p)$ and the radiation mode $\nu=(\omega,\beta,m,p)$, respectively. Their expressions are

$$G_{\mu eg}=\sqrt{\frac{\omega\beta'}{4\pi\epsilon_0\hbar}}(\mathbf{d}_{eg}\cdot\mathbf{e}^{(\mu)})e^{i(f\beta z+p\varphi)},$$

$$G_{\nu eg}=\sqrt{\frac{\omega}{4\pi\epsilon_0\hbar}}(\mathbf{d}_{eg}\cdot\mathbf{e}^{(\nu)})e^{i(\beta z+m\varphi)}. \quad (9)$$

III. CHARACTERISTICS OF SPONTANEOUS EMISSION

The solutions to the Heisenberg equations for the photon operators a_μ and a_ν can be written as

$$a_\mu(t)=a_\mu(t_0)+\sum_{eg}G^*_{\mu eg}\int_{t_0}^{t}dt'\sigma_{ge}(t')e^{i(\omega-\omega_0)t'},$$

$$a_\nu(t)=a_\nu(t_0)+\sum_{eg}G^*_{\nu eg}\int_{t_0}^{t}dt'\sigma_{ge}(t')e^{i(\omega-\omega_0)t'}. \quad (10)$$

Assume that the field is initially in the vacuum state. Since the continuum of the guided and radiation modes is broadband around the atomic frequency, the Markoff approximation $\sigma_{ge}(t')=\sigma_{ge}(t)$ can be applied to describe the back action of the second terms in Eqs. (10) on the atom. We neglect the vacuum frequency shifts. Then, for the atomic operators $\sigma_{ij}=|i\rangle\langle j|$, we obtain the Heisenberg-Langevin equations

$$\dot{\sigma}_{ge}=-\frac{1}{2}\sum_{e'}\Gamma_{ee'}\sigma_{ge'}+\hat{\xi}_{ge},$$

$$\dot{\sigma}_{ee'}=-\frac{1}{2}\sum_{e''}(\Gamma_{e'e''}\sigma_{ee''}+\Gamma_{e''e}\sigma_{e''e'})+\hat{\xi}_{ee'},$$

$$\dot{\sigma}_{gg'}=\sum_{ee'}\Gamma_{ee'gg'}\sigma_{ee'}+\hat{\xi}_{gg'}. \quad (11)$$

Here the coefficients

$$\Gamma_{ee'}=\gamma^{(\mathrm{g})}_{ee'}+\gamma^{(\mathrm{r})}_{ee'},$$

$$\Gamma_{ee'gg'}=\gamma^{(\mathrm{g})}_{ee'gg'}+\gamma^{(\mathrm{r})}_{ee'gg'} \quad (12)$$

characterize the total spontaneous emission and ξ_{ij} are the noise operators. The coefficients $\gamma^{(\mathrm{g})}_{ee'}$ and $\gamma^{(\mathrm{g})}_{ee'gg'}$ describe spontaneous emission into guided modes. They are given by $\gamma^{(\mathrm{g})}_{ee'}=2\pi\Sigma_{fpg}G_{\mu_0 eg}G^*_{\mu_0 e'g}$ and $\gamma^{(\mathrm{g})}_{ee'gg'}=2\pi\Sigma_{fp}G_{\mu_0 eg}G^*_{\mu_0 e'g'}$, where $\mu_0=(\omega_0,f,p)$. The coefficients $\gamma^{(\mathrm{r})}_{ee'}$ and $\gamma^{(\mathrm{r})}_{ee'gg'}$ describe spontaneous emission into radiation modes. They are given by $\gamma^{(\mathrm{r})}_{ee'}=2\pi\Sigma_{mpg}\int_{-k_0n_2}^{k_0n_2}d\beta\,G_{\nu_0 eg}G^*_{\nu_0 e'g}$ and $\gamma^{(\mathrm{r})}_{ee'gg'}=2\pi\Sigma_{mp}\int_{-k_0n_2}^{k_0n_2}d\beta\,G_{\nu_0 eg}G^*_{\nu_0 e'g'}$, where $\nu_0=(\omega_0,\beta,m,p)$. We find the relations

$$\gamma^{(\mathrm{g})}_{ee'}=\sum_g\gamma^{(\mathrm{g})}_{ee'gg},$$

$$\gamma^{(\mathrm{r})}_{ee'}=\sum_g\gamma^{(\mathrm{r})}_{ee'gg}. \quad (13)$$

In terms of the spherical tensor components [13] $d^{(l)}_{eg}$, $e^{(\mu_0)}_l$, and $e^{(\nu_0)}_l$ of the vectors $\mathbf{d}_{eg}$, $\mathbf{e}^{(\mu_0)}$, and $\mathbf{e}^{(\nu_0)}$, respectively, we obtain

$$\gamma^{(\mathrm{g})}_{ee'gg'}=\sum_{l,l'=0,\pm1}(-1)^{l+l'}d^{(l)}_{eg}d^{(l')*}_{e'g'}U^{(\mathrm{g})}_{-l,-l'},$$

$$\gamma^{(\mathrm{r})}_{ee'gg'}=\sum_{l,l'=0,\pm1}(-1)^{l+l'}d^{(l)}_{eg}d^{(l')*}_{e'g'}U^{(\mathrm{r})}_{-l,-l'}, \quad (14)$$

where

$$U^{(\mathrm{g})}_{ll'}=\frac{\omega_0\beta'_0}{2\epsilon_0\hbar}\sum_{fp}e^{(\mu_0)}_l e^{(\mu_0)*}_{l'},$$

$$U^{(\mathrm{r})}_{ll'}=\frac{\omega_0}{2\epsilon_0\hbar}\sum_{mp}\int_{-k_0n_2}^{k_0n_2}d\beta\,e^{(\nu_0)}_l e^{(\nu_0)*}_{l'}. \quad (15)$$

Equations (12)–(15) together with the mode functions $\mathbf{e}^{(\mu)}$ and $\mathbf{e}^{(\nu)}$, given in Appendixes A and B, respectively, constitute explicit expressions for the decay parameters of atomic populations as well as atomic coherences. These equations as well as the Heisenberg-Langevin equations (11) are the key analytical results of our paper.

Note that, due to the selection rules, the spherical tensor component $d^{(l)}_{eg}$ is nonzero only for $l=M_e-M_g$. On the other hand, due to the cylindrical symmetry, the functions $U^{(\mathrm{g})}_{ll'}$ and $U^{(\mathrm{r})}_{ll'}$ are zero for $(l=0,l'=\pm1)$ and $(l=\pm1,l'=0)$. Hence, $\gamma^{(\mathrm{g})}_{ee'}$ and $\gamma^{(\mathrm{r})}_{ee'}$ are nonzero only for $M_{e'}=M_e,M_e\pm2$. The parameters $\gamma^{(\mathrm{g})}_{ee}$ and $\gamma^{(\mathrm{r})}_{ee}$ describe the spontaneous emission from the excited magnetic sublevel $|e\rangle=|F'=5M'\rangle$ with $M'=M_e$ into guided and radiation modes, respectively. When we use the symmetry properties of the mode functions, we find

$$\gamma^{(\mathrm{g})}_{ee}=\frac{2\omega_0\beta'_0}{\epsilon_0\hbar}\sum_g|(\mathbf{d}_{eg}\cdot\mathbf{e}^{(\omega_0,+,+)})|^2,$$

$$\gamma^{(\mathrm{r})}_{ee}=\frac{2\omega_0}{\epsilon_0\hbar}\sum_g\sum_m\int_0^{k_0n_2}d\beta\,|(\mathbf{d}_{eg}\cdot\mathbf{e}^{(\omega_0,\beta,m,+)})|^2. \quad (16)$$

Here $\mathbf{e}^{(\omega_0,+,+)}$ is the mode function of the fundamental guided mode $\mu=(\omega,f,p)$ with $\omega=\omega_0$ (atomic resonant frequency), $f=+$ (forward direction), and $p=+$ (counterclockwise polarization), while $\mathbf{e}^{(\omega_0,\beta,m,+)}$ is the mode function of the radiation mode $\nu=(\omega,\beta,m,p)$ with the frequency $\omega=\omega_0$ and the polarization $p=+$. The total decay rate of the population of $|e\rangle$ is

$$\Gamma_{ee}=\gamma^{(\mathrm{g})}_{ee}+\gamma^{(\mathrm{r})}_{ee}. \quad (17)$$

The summation over the lower-sublevel index g in Eqs. (16) is a consequence of the fact that the decay rate of the population of an arbitrary level is the sum of the decay rates of the associated downward transitions. The magnitudes and orientations of the dipoles of the partial transitions are determined by the quantum numbers. They can not be arbitrary.

They are different from each other. To calculate the population decay rate of a level of a specific realistic atom, we need to calculate and sum up the decay rates of the associated downward transitions using the quantum numbers of the specific atomic level structure. Due to the split into and summation over the partial transitions, whose dipoles are complex and differing in magnitude and orientation, the typical absolute and relative magnitudes of the population decay rate of a realistic multilevel atom can be substantially different from that for the case of a two-level atom. This is the essence of our treatment as well as most other treatments for the population decay rates of realistic multilevel atoms. In addition, off-diagonal elements such as $\Gamma_{ee'}$ with $e \neq e'$ and $\Gamma_{ee'gg'}$ with $e \neq e'$ or $g \neq g'$ do not exist in the case of two-level atoms. They describe the decay of cross-level coherences and arise only in the framework of a multilevel-atom model. The knowledge of both diagonal and off-diagonal types of decay characteristics is important for the studies of absorption and emission properties of the multilevel atom [7].

Our formalism allows the atom to be inside or outside the fiber. It also allows the atom to have, in principle, an arbitrary level structure. Our results, when reduced to the case of a two-level atom inside or outside a passive fiber, are in perfect agreement with other studies [3,4]. The agreement with the results of Ref. [3] has been confirmed analytically and numerically. The agreement with the results of Ref. [4] has been checked numerically. For a multilevel atom in free space, we again have agreement with the previous results [7]. Henceforth, as a typical example, we focus our attention only to the case of a cesium atom in the outside of a thin fiber.

IV. NUMERICAL RESULTS

In what follows, we demonstrate the results of our numerical calculations for the decay characteristics of magnetic sublevels of a cesium atom in the presence of a thin fiber. For simplicity, we show only the numerical results for the diagonal decay coefficients, which describe the rates of population decay. We do not present the numerical results for the off-diagonal decay coefficients because we cannot gain much insight from showing them graphically. However, we emphasize that these parameters can be easily calculated from Eqs. (12)–(15) and that the knowledge of these parameters is important for investigating the dynamics of cesium atoms interacting with guided fields.

We plot in Fig. 2 the spatial dependence of the spontaneous emission rates for various magnetic sublevels $6P_{3/2}F'=5M'$ into guided modes, radiation modes, and both types of modes. The fiber radius a is chosen to be 200 nm, which is in the optimal range for producing optical trapping potentials [10,11]. According to Fig. 2, different magnetic sublevels of the same state $6P_{3/2}$ have different decay rates in the vicinity of the fiber surface, unlike the case of atomic cesium in free space. The presence of the fiber produces substantial decay rates into guided modes. Indeed, when the atom is positioned on the fiber surface, the decay rates into guided modes $\gamma_{ee}^{(g)}$ vary from $0.31\Gamma_0$ for $M_e=0$ to $0.48\Gamma_0$ for $M_e=\pm 5$ [see Fig. 2(a)]. Here $\Gamma_0=33\times 10^6\ \mathrm{s}^{-1}$ is the decay rate of the cesium state $6P_{3/2}$ in free space. In addition, the

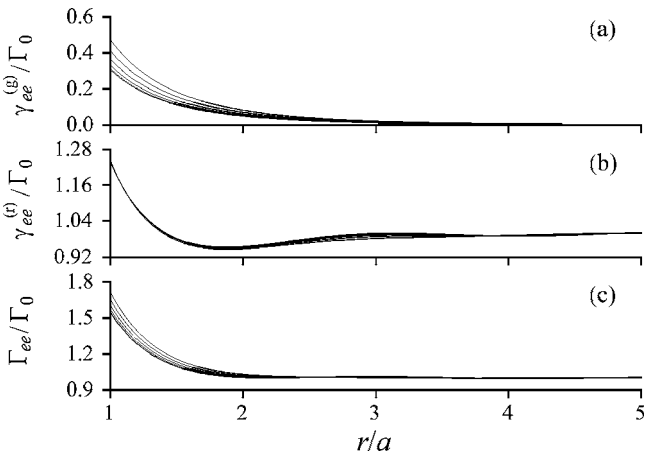

FIG. 2. Spontaneous emission rates for various magnetic sublevels $6P_{3/2}F'=5M'$ into (a) guided modes, (b) radiation modes, and (c) both types of modes as functions of the position of the atom. Different lines in each plot correspond to different values $|M'|=0$, 1, 2, 3, 4, and 5. The fiber radius is $a=200$ nm. The wavelength of the atomic transition is $\lambda_0=852$ nm. The refractive indices of the fiber and the vacuum clad are $n_1=1.45$ and $n_2=1$, respectively. The rates are normalized to the free-space decay rate Γ_0.

decay rates into radiation modes $\gamma_{ee}^{(r)}$ and the total decay rates Γ_{ee} are enhanced from the free-space rate Γ_0 by small factors. The maximal values of $\gamma_{ee}^{(r)}/\Gamma_0$ and Γ_{ee}/Γ_0 are around 1.2 and 1.6, respectively [see Figs. 2(b) and 2(c)]. As expected, the effect of the fiber on the decay rates is largest for the atom on the fiber surface. When the atom is far away from the fiber, $\gamma_{ee}^{(g)}$ reduces to zero while $\gamma_{ee}^{(r)}$ and Γ_{ee} approach the free-space value Γ_0. The small oscillations around the value of unity in Fig. 2(b) can be ascribed to the constructive/destructive interference due to reflections from the fiber surface [3]. Note that the decay rates of the sublevels M_e and $-M_e$ are the same. Therefore, the maximum number of lines in each plot is six. However, since the difference between the decay rates for $M_e=0$ and $|M_e|=1$ is very small, we can distinguish only five lines in each plot of Fig. 2.

In Fig. 3, we plot the spontaneous emission rates for various magnetic sublevels as functions of the fiber size parameter k_0a for the atom on the fiber surface. The separation between the curves in the figure confirms again that different magnetic sublevels have different decay rates due to the presence of the fiber. We observe that, in the shown range of k_0a, the decay rates into guided modes $\gamma_{ee}^{(g)}$ have a maximum [see Fig. 3(a)], while, depending on the magnetic sublevels, the decay rates into radiation modes $\gamma_{ee}^{(r)}$ have one or two minima [see Fig. 3(b)]. Such a behavior indicates that there can exist an optimal value of the fiber size parameter for which the fraction of decay due to guided modes reaches its largest value [see also Fig. 4(b) below]. The overall behavior of the curves in Fig. 3(c) implies that the total decay is less sensitive to k_0a as compared to that for the guided modes.

In order to get deeper insight into the decay into guided modes, we plot the ratio $\gamma_{ee}^{(g)}/\Gamma_{ee}$ for various magnetic sublevels in Figs. 4(a) and 4(b) as a function of r/a and k_0a, respectively. We observe from Fig. 4(a) that, in the close vicinity of the fiber surface, the fractional decay rates into

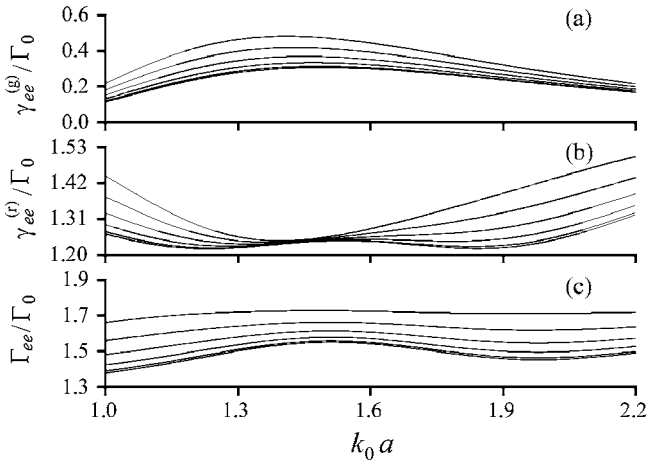

FIG. 3. Spontaneous emission rates for various magnetic sublevels into (a) guided modes, (b) radiation modes, and (c) both types of modes as functions of the fiber radius. The atom is located on the fiber surface. Other parameters are as in Fig. 2.

guided modes are substantial, in the range from 0.2 (for $M_e=0$) to 0.28 (for $M_e=\pm 5$). With increasing distance of the atom from the surface, $\gamma_{ee}^{(g)}/\Gamma_{ee}$ quickly reduces to zero, as expected. As can be seen from Fig. 4(b), $\gamma_{ee}^{(g)}/\Gamma_{ee}$ is sensitive to $k_0 a$, reaching a maximum at around $k_0 a=1.45$. This size parameter corresponds to a fiber radius of about 200 nm, which is in the optimal range for producing optical trapping potentials [10,11]. For such a parameter, a significant fraction (up to 28% for $M_e=\pm 5$) of spontaneous emission by the atom can be channeled into guided modes. The above maximal value, obtained for a cesium atom, is substantially smaller than the corresponding value for a two-level atom with radial dipole [4]. Such a reduction is a consequence of the degeneracy of the ground state of cesium as well as the complexity of its dipole. Indeed, the dipoles of the partial transitions are complex and differing in magnitude and orientation. Therefore, the results for cesium do not correspond to the results for a two-level atom with a specific real radial, axial, or tangential dipole.

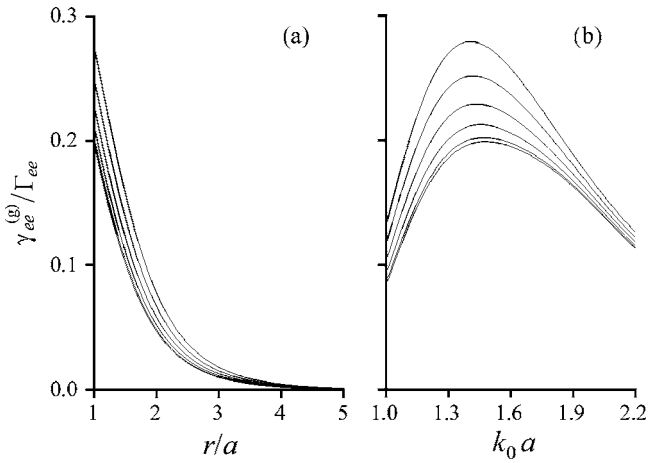

FIG. 4. Fractional decay rates for various magnetic sublevels into guided modes as functions of (a) the atomic position and (b) the fiber radius with the atom on the fiber surface. Other parameters are as in Fig. 2. Note that the peaks in (b) occur around $k_0 a=1.45$, which correspond to $a=200$ nm for the cesium D_2 line.

V. SUMMARY

In conclusion, we have studied the spontaneous emission by a cesium atom in the vicinity of a subwavelength-diameter fiber. We have shown that the confinement of the guided modes and the degeneracy of the magnetic sublevels play an important role in deciding the spontaneous emission from the cesium atom. When the fiber radius is about 200 nm, the fractional decay rates into guided modes can be significant (up to 28%). Our results for this realistic "atom + fiber" system can be used for future experiments on generating and guiding a few photons along a thin fiber. They may also find applications as atom nanoprobes as well as efficient subwavelength fiber couplers.

ACKNOWLEDGMENTS

This work was carried out under the 21st Century COE program on "Coherent Optical Science."

APPENDIX A: MODE FUNCTIONS OF THE FUNDAMENTAL GUIDED MODES

For the guided modes, the longitudinal propagation constant β is determined by the fiber eigenvalue equation [15]

$$\frac{J_0(ha)}{haJ_1(ha)} = -\frac{n_1^2+n_2^2}{2n_1^2}\frac{K_1'(qa)}{qaK_1(qa)} + \frac{1}{h^2a^2} - \left\{\left[\frac{n_1^2-n_2^2}{2n_1^2}\frac{K_1'(qa)}{qaK_1(qa)}\right]^2 + \frac{\beta^2}{n_1^2k^2}\left(\frac{1}{q^2a^2}+\frac{1}{h^2a^2}\right)^2\right\}^{1/2}. \quad \text{(A1)}$$

Here the parameters $h=(n_1^2k^2-\beta^2)^{1/2}$ and $q=(\beta^2-n_2^2k^2)^{1/2}$ characterize the fields inside and outside the fiber, respectively. The notation J_n and K_n stand for the Bessel functions of the first kind and the modified Bessel functions of the second kind, respectively.

The mode functions of the electric parts of the fundamental guided modes [15] are given, for $r<a$, by

$$e_r^{(\mu)} = iA\frac{q}{h}\frac{K_1(qa)}{J_1(ha)}[(1-s)J_0(hr)-(1+s)J_2(hr)],$$

$$e_\varphi^{(\mu)} = -pA\frac{q}{h}\frac{K_1(qa)}{J_1(ha)}[(1-s)J_0(hr)+(1+s)J_2(hr)],$$

$$e_z^{(\mu)} = fA\frac{2q}{\beta}\frac{K_1(qa)}{J_1(ha)}J_1(hr), \quad \text{(A2)}$$

and, for $r>a$, by

$$e_r^{(\mu)} = iA[(1-s)K_0(qr)+(1+s)K_2(qr)],$$

$$e_\varphi^{(\mu)} = -pA[(1-s)K_0(qr)-(1+s)K_2(qr)],$$

$$e_z^{(\mu)} = fA\frac{2q}{\beta}K_1(qr). \tag{A3}$$

Here, the parameter s is defined as $s=(1/q^2a^2+1/h^2a^2)/[J_1'(ha)/haJ_1(ha)+K_1'(qa)/qaK_1(qa)]$, and the coefficient A is determined from the normalization condition.

To normalize the guided mode functions, we need to calculate the constant

$$N_\mu = \int_0^{2\pi} d\varphi \int_0^\infty n_{\rm rf}^2 |\mathbf{e}^{(\mu)}|^2 r dr. \tag{A4}$$

We find

$$N_\mu = 2\pi A^2 a^2 (n_1^2 P_1 + n_2^2 P_2), \tag{A5}$$

where

$$P_1 = \frac{q^2K_1^2(qa)}{h^2J_1^2(ha)}\left\{(1-s)^2[J_0^2(ha)+J_1^2(ha)] + (1+s)^2[J_2^2(ha) - J_1(ha)J_3(ha)] + 2\frac{h^2}{\beta^2}[J_1^2(ha) - J_0(ha)J_2(ha)]\right\} \tag{A6}$$

and

$$P_2 = (1-s)^2[K_1^2(qa) - K_0^2(qa)] + (1+s)^2[K_1(qa)K_3(qa) - K_2^2(qa)] + 2\frac{q^2}{\beta^2}[K_0(qa)K_2(qa) - K_1^2(qa)]. \tag{A7}$$

APPENDIX B: MODE FUNCTIONS OF THE RADIATION MODES

For the radiation modes, we have $-kn_2<\beta<kn_2$. The characteristic parameters for the field in the inside and outside of the fiber are $h=\sqrt{k^2n_1^2-\beta^2}$ and $q=\sqrt{k^2n_2^2-\beta^2}$, respectively. The mode functions of the electric parts of the radiation modes [15] are given, for $r<a$, by

$$e_r^{(\nu)} = \frac{i}{h^2}\left[\beta hAJ_m'(hr) + im\frac{\omega\mu_0}{r}BJ_m(hr)\right],$$

$$e_\varphi^{(\nu)} = \frac{i}{h^2}\left[im\frac{\beta}{r}AJ_m(hr) - h\omega\mu_0 BJ_m'(hr)\right],$$

$$e_z^{(\nu)} = AJ_m(hr), \tag{B1}$$

and, for $r>a$, by

$$e_r^{(\nu)} = \frac{i}{q^2}\sum_{j=1,2}\left[\beta qC_jH_m^{(j)\prime}(qr) + im\frac{\omega\mu_0}{r}D_jH_m^{(j)}(qr)\right],$$

$$e_\varphi^{(\nu)} = \frac{i}{q^2}\sum_{j=1,2}\left[im\frac{\beta}{r}C_jH_m^{(j)}(qr) - q\omega\mu_0 D_jH_m^{(j)\prime}(qr)\right],$$

$$e_z^{(\nu)} = \sum_{j=1,2} C_jH_m^{(j)}(qr). \tag{B2}$$

The coefficients C_j and D_j are related to the coefficients A and B as [3]

$$C_j = (-1)^j\frac{i\pi q^2 a}{4n_2^2}(AL_j + i\mu_0 cBV_j),$$

$$D_j = (-1)^{j-1}\frac{i\pi q^2 a}{4}(i\epsilon_0 cAV_j - BM_j), \tag{B3}$$

where

$$V_j = \frac{mk\beta}{ah^2q^2}(n_2^2-n_1^2)J_m(ha)H_m^{(j)*}(qa),$$

$$M_j = \frac{1}{h}J_m'(ha)H_m^{(j)*}(qa) - \frac{1}{q}J_m(ha)H_m^{(j)*\prime}(qa),$$

$$L_j = \frac{n_1^2}{h}J_m'(ha)H_m^{(j)*}(qa) - \frac{n_2^2}{q}J_m(ha)H_m^{(j)*\prime}(qa). \tag{B4}$$

We specify two polarizations by choosing $B=i\eta A$ and $B=-i\eta A$ for $p=+$ and $p=-$, respectively. The orthogonality of the modes requires

$$\int_0^{2\pi} d\varphi \int_0^\infty n_{\rm rf}^2 [\mathbf{e}^{(\nu)}\mathbf{e}^{(\nu')*}]_{\beta=\beta',m=m'} r dr = N_\nu \delta_{pp'}\delta(\omega-\omega'). \tag{B5}$$

This leads to

$$\eta = \epsilon_0 c\sqrt{\frac{n_2^2|V_j|^2 + |L_j|^2}{|V_j|^2 + n_2^2|M_j|^2}}. \tag{B6}$$

The normalization constant N_ν is given by

$$N_\nu = \frac{8\pi\omega}{q^2}\left(n_2^2|C_j|^2 + \frac{\mu_0}{\epsilon_0}|D_j|^2\right). \tag{B7}$$

[1] S. A. Maier *et al.*, Nat. Mater. **2**, 229 (2003); T. W. Ebbesen *et al.*, Nature (London) **391**, 667 (1998).

[2] H. Nha and W. Jhe, Phys. Rev. A **56**, 2213 (1997).

[3] T. Søndergaard and B. Tromborg, Phys. Rev. A **64**, 033812 (2001).

[4] V. V. Klimov and M. Ducloy, Phys. Rev. A **69**, 013812 (2004).

[5] See, for example, *Cavity Quantum Electrodynamics*, edited by P. R. Berman (Academic, New York, 1994); *Optical Processes in Microcavities*, edited by R. Chang and A. Campillo (World Scientific, Singapore, 1996).

[6] V. V. Klimov, M. Ducloy, and V. S. Letokhov, Eur. Phys. J. D **20**, 133 (2002).

[7] See S. Chang and V. Minogin, Phys. Rep. **365**, 65 (2002), and the references therein.

[8] S. Chu, Rev. Mod. Phys. **70**, 685 (1998); C. Cohen-Tannoudji, *ibid.* **70**, 707 (1998); W. D. Phillips, *ibid.* **70**, 721 (1998).

[9] C. S. Adams, M. Sigel, and J. Mlynek, Phys. Rep. **240**, 143 (1994); V. I. Balykin and V. S. Letokhov, *Atom Optics with Laser Light*, Vol. 18 of *Laser Science and Technology* (Harwood Academic, New York, 1995), p. 115; P. Meystre, *Atom Optics* (Springer, New York, 2001), p. 311.

[10] V. I. Balykin, K. Hakuta, F. L. Kien, J. Q. Liang, and M. Morinaga, Phys. Rev. A **70**, 011401(R) (2004).

[11] Fam Le Kien, V. I. Balykin, and K. Hakuta, Phys. Rev. A **70**, 063403 (2004).

[12] H. J. Metcalf and P. van der Straten, *Laser Cooling and Trapping* (Springer, New York, 1999).

[13] See, for example, B. W. Shore, *The Theory of Coherent Atomic Excitation* (Wiley, New York, 1990).

[14] C. M. Caves and D. D. Crouch, J. Opt. Soc. Am. B **4**, 1535 (1987); K. J. Blow, R. Loudon, S. J. D. Phoenix, and T. J. Shepherd, Phys. Rev. A **42**, 4102 (1990); P. Domokos, P. Horak, and H. Ritsch, *ibid.* **65**, 033832 (2002).

[15] See, for example, D. Marcuse, *Light Transmission Optics* (Krieger, Malabar, FL, 1989); A. W. Snyder and J. D. Love, *Optical Waveguide Theory* (Chapman and Hall, New York, 1983).